Geosci. Model Dev. Discuss., 5, 309–346, 2012
www.geosci-model-dev-discuss.net/5/309/2012/
doi:10.5194/gmdd-5-309-2012

Geoscientific Model Development Discussions

Assimilation of OMI NO_2 retrievals into the limited-area chemical transport model DEHM (V2007.0) with a 2-D OI algorithm

J. D. Silver[1], J. Brandt[1], M. Hvidberg[2], and J. Frydendall[3]

[1]Department of Environmental Science, Aarhus University, Frederiksborgvej 399, 4000 Roskilde, Denmark
[2]National Survey and Cadastre, Danish Ministry of the Environment, Rentemestervej 8, 2400 Copenhagen NV, Denmark
[3]Institute of Mathematical Modelling, Danish Technical University, Richard Petersens Plads, Building 321, 2800 Lyngby, Denmark

Received: 19 January 2012 – Accepted: 26 January 2012 – Published: 13 February 2012

Correspondence to: J. D. Silver (jds@dmu.dk)

Published by Copernicus Publications on behalf of the European Geosciences Union.

Abstract

Data assimilation is the process of combining real-world observations with a modelled geophysical field. The increasing abundance of satellite retrievals of atmospheric trace gases makes chemical data assimilation a powerful tool for improving air quality forecasts.

We implemented a two-dimensional optimal interpolation (OI) algorithm to assimilate satellite-derived estimates of tropospheric NO_2 column concentrations into the Danish Eulerian Hemispheric Model (DEHM, version V2007.0), a three-dimensional, European-scale, chemical transport model. In particular, we describe how we used observational data to estimate the background error covariance matrix, **B**. In the assimilation, the tropospheric column NO_2 field was adjusted and the modelled NO_2 profile was scaled accordingly; other species were only adjusted indirectly via changes to NO_2 concentrations.

We ran a number of experiments to compare different parameterisations of **B**; this involved varying the length scale used in **B**, the relative weighting of the background and observation errors, the errors assigned to observations and the influence of clustered observations. We assessed model performance by comparing the analysed fields to an independent set of observations: ground-based measurements of NO_2 concentrations. Ozonosonde profiles were also used for verification.

The analysed NO_2 and O_3 concentrations were more accurate than those from a reference simulation without assimilation, with lower bias for both species and improved correlation for NO_2. The experiments showed that appropriately chosen parameters for the **B** matrix, estimated using innovation statistics, yielded more accurate surface NO_2 concentrations. There was good agreement between the seasonally-averaged observed and modelled O_3 profiles.

The simple OI scheme was effective and computationally feasible in this context, where only a single species was assimilated and only a two-dimensional field was adjusted. However there are certain limitations to using this assimilation scheme for

GMDD

5, 309–346, 2012

more highly multi-dimensional problems. Although forecast accuracy was not examined here, we discuss the potential for improving NO_2 forecasts by using assimilation to generate initial conditions.

1 Introduction

Chemical transport models (CTMs) are widely used for forecasting air pollution, evaluating proposed emission reductions, studying chemical or physical processes, and assessing climate-scale effects and forcings related to atmospheric components (Jacobson, 2005). Modelled concentrations are often highly uncertain, and can be improved in several ways, such as better parameterisation of sub-grid scale processes, more accurate estimates of forcings at the lateral and lower boundary conditions, higher spatial resolution, higher order numerical methods, and more accurate initial conditions. Data assimilation (DA) aims to improve estimates of initial conditions by combining previous forecasts with recent observations (Kalnay, 2003).

In recent decades, satellite retrievals of atmospheric constituents have complemented observations from ground-based monitoring stations (Martin, 2008). Satellite retrievals provide concentration estimates for the total vertical column, for a partial column (e.g. the troposphere) or at a range of vertical levels, and they cover a far greater geographical range across the planet compared to ground-based measurements of surface concentrations. They therefore present great potential for use in "chemical DA" (i.e. DA for CTMs). For a comprehensive review of chemical DA, see Carmichael et al. (2008).

Optimal interpolation (OI) is the one of simplest DA algorithm currently applied to CTMs; it is based on a least-squares formulation of the DA problem. While the assumptions underpinning OI are relatively crude, this algorithm is simple to implement and may be computationally cheaper than other more sophisticated DA methods, provided that neither the number of observations nor the number of model variables is too large. In meteorology, OI has long been surpassed by variational or Kalman filtering

GMDD
5, 309–346, 2012

methods (Kalnay, 2003), however it is still in use with chemical transport models. For example, Mok et al. (2008) used OI with a Gaussian puff model for sulfur dioxide over Lisbon, Portugal. Adhikary et al. (2008) and Matsui et al. (2004) applied OI to assimilate satellite retrievals of aerosol optical depth when modelling aerosol concentrations over South-East Asia and the eastern United States, respectively.

In the case of off-line CTMs, a small perturbation in the initial conditions will typically decay as the simulation proceeds, mainly due to forcing from sources and sinks such as chemistry and emissions (Carmichael et al., 2008; Wu et al., 2008). Thus the quality of the initial conditions is less critical in air quality modelling than for numerical weather prediction (NWP) models, where perturbations tend to grow with time. In the case of short-lived chemical species, the duration of the initial perturbation may be quite brief (e.g. one day) and this limits the extent to which better initial conditions can improve concentrations forecasts. Chemical DA can, nonetheless, be used for historical reanalysis.

The conceptual and practical simplicity of OI makes the algorithm a reasonable starting point for use of DA in CTMs. Wu et al. (2008) compared four different DA methods (OI, two types of Kalman filter, and four-dimensional variational assimilation) applied to ozone forecasting. They demonstrated that OI, although a relatively simple method, was comparable in performance to the more advanced and computationally intensive variational and Kalman filter methods.

This study concerns the assimilation of satellite-derived estimates of tropospheric concentrations of nitrogen dioxide (NO_2). NO_2 plays an important role in atmospheric chemistry. In the stratosphere, it is involved in catalytic cycles that destroy ozone (O_3); in the troposphere NO_2 is a key O_3 precursor, especially in polluted urban environments (Seinfeld and Pandis, 2006, chapters 5, 6). O_3 is itself an important precursor for the hydroxyl radical, a key atmospheric oxidant (Jacob, 1999). NO_2 photo-dissociates into NO and O for wavelengths less than 370 nm, and it can be responsible for reduced visibility in polluted environments. The principal anthropogenic source of NO_x ($NO_2 + NO$) is combustion, and the main removal mechanism is conversion to HNO_3,

GMDD
5, 309–346, 2012

which deposits rapidly. NO and NO_2 inter-convert and atmospheric lifetime of NO_x varies from hours to days at the surface to a couple of weeks in the upper troposphere (Seinfeld and Pandis, 2006, pp. 224). There is also substantial seasonal variation; Schaub et al. (2007) estimated the lifetime of NO_x to be around 3 h during summer and 13 h during winter. Thus NO_2 is a relatively "local" pollutant.

NO_2 is also of interest from a human health perspective. For example, exposure to NO_2 has been linked to reduced lung function, asthma and increased mortality (Peters et al., 1999; Belanger et al., 2006; Stieb et al., 2002). Furthermore, NO_2 is a precursor of NO_3^- ions, which can be an important component of particulate matter (PM); PM has also been associated with numerous adverse impacts on human health (Pope, 2000). In urban environments, NO_2 and PM concentrations are typically highly correlated, since combustion processes are the main anthropogenic emission sources for both pollutants. This makes it difficult to separate the independent health impacts of NO_2 and PM in an epidemiological context, especially since there is a poor correlation between measured personal exposure and ambient concentrations observed at fixed monitoring sites (Searl, 2004). See WHO (2003) or Searl (2004) for reviews of the health effects of NO_2 exposure.

In this study we make use of tropospheric NO_2 column concentrations, derived from measurements by the Ozone Monitoring Instrument (OMI) aboard the NASA satellite AURA (see Sect. 2.1). These NO_2 retrievals have been used in a number of contexts. They have been used to re-estimate NO_x emission rates (Zhao and Wang, 2009). They have been validated against ground-based measurements (Lamsal et al., 2008), spectrometers (Ionov et al., 2006), aircraft campaigns (Boersma et al., 2008). They are a resource for validation of air quality models (Huijnen et al., 2010) or comparison with retrievals from other satellites (Boersma et al., 2008). Furthermore, they have be used to study particular pollution or emission reduction events (Wang et al., 2007). Wang et al. (2011) assimilated OMI NO_2 retrievals in a regional CTM, and we will compare our findings with those of Wang et al. (2011) in Sect. 5.

GMDD
5, 309–346, 2012

The present study follows from the work of Frydendall et al. (2009), who assimilated in-situ O_3 measurements using OI in a three-layer, regional CTM (DEOM; Brandt et al., 2001a). They compared O_3 fields, calculated with or without DA, to observations from ground-based monitoring stations. Several variants of this DA algorithm were trialled, and optimised for the available observations (namely, O_3 measurements from ground-level monitoring stations).

In this article, we assimilated retrieved tropospheric NO_2 columns from OMI. We applied OI to a more advanced CTM than the one used by Frydendall et al. (2009) (see Sect. 2.2). We describe how the background error covariance matrix was parameterised based on the satellite innovation statistics (Hollingsworth and Lonnberg, 1986); we account for the fact that observations are asynchronous and from a single mobile observing platform (see Sects. 2.3 and 2.4). We present the results of experiments in which we tested different parameterisations of the modelling/assimilation setup in order to optimise its performance for the available data (see Sect. 3.1). The analysed concentration fields are compared to ground-based observations of NO_2 concentrations (see Sects. 3.2 and 4). In Sect. 5, we discuss these results in the broader context of forecasting and chemical DA.

2 Assimilation and modelling framework

2.1 OMI retrievals

Tropospheric NO_2 concentrations were retrieved from radiances measured by the Dutch-Finnish Ozone Monitoring Instrument (OMI) aboard the NASA satellite Aura. Aura's orbit is sun-synchronous, crossing the equator between 13:30 and 14:00 local time, passing over Europe shortly after. The retrieval scheme is described in Boersma et al. (2002, 2007). Retrievals from regions with cloud cover, or otherwise deemed unreliable by the retrieval algorithm, were excluded, as were negative estimates of concentrations (which are an artifact of the retrieval scheme). We used version 1.0.2

GMDD
5, 309–346, 2012

(released 29 April 2008) of the level 2 retrieved tropospheric column NO_2 concentrations. The retrieval process yielded a measure of the estimate's uncertainty. The retrieved total column was found to be highly correlated with the associated uncertainty measure ($R^2 = 0.95$).

The OMI data represent a different temporal and spatial resolution compared to that of the CTM used in this study (see Sect. 2.2). The model domain covered Europe, and satellite readings in this area were available several times a day, usually few hours before and after 12:00 UTC. Multiple images are produced per satellite overpass. The spatial resolution of the CTM used in this study is approximately 50 km × 50 km across the model domain. Resolution of the OMI images varies across the camera's swath. Nadir pixels are 13 km × 24 km, while pixels furthest from nadir are 13 km × 128 km. Very few, if any, OMI pixels larger than 50 km are used in the present work.

In a given image, many pixels were deemed to be unreliable, mainly due to clouds. Often as much as 50 % pixels were classified as unreliable. Such pixels are excluded from any further processing in the work presented here.

2.2 Chemical transport model: DEHM

The Danish Eulerian Hemispheric Model (DEHM) is an off-line, Eulerian, three-dimensional, long-range CTM (Christensen, 1997; Brandt et al., 2001a,b,c; Frohn et al., 2002). The model simulates atmospheric transport and diffusion, chemical transformations, wet and dry deposition, and emissions from a range of biogenic and anthropogenic sources.

Version V2007.0 of DEHM was used in this study: this is the version developed for the 2007 annual report for the Danish Air Quality Monitoring Programme (NOVANA; Kemp et al., 2008). In the present configuration of the model, the horizontal domain covers Europe (Fig. 1), spatially discretised with a 96 × 96 horizontal grid using a polar stereographic projection. In the vertical, the model extends from the surface to 100 hPa in 20 vertical layers using terrain-following σ-coordinates. This version of the model describes a total of 58 gaseous chemical species and 5 classes of particulate

GMDD
5, 309–346, 2012

matter. The chemistry scheme is similar to that used in the European Monitoring and Evaluation Programme (EMEP) model (Simpson et al., 2003). Meteorological variables (e.g. wind speed, temperature, pressure) were calculated by the Eta mesoscale numerical weather prediction model (Black, 1994; Janjic, 1990, 1994), with initial conditions provided by NCEP FNL (Final) Operational Global Analysis data set (available at http://dss.ucar.edu). Emission rates were based on the following emissions inventories: EMEP (Vestreng and Klein, 2002), EDGAR (Olivier and Berdowski, 2001), GEIA (Benkovitz et al., 1996) and RETRO (Schultz et al., 2007).

The extended continuity equation is split into several sub-equations, which are in turn solved sequentially (Lanser and Verwer, 1999). Horizontal advection is solved via "accurate space derivatives" (Dardub and Seinfeld, 1994), and by applying Forester and Bartnicki filters to resolve, respectively, spurious oscillations and negative mass (Forester, 1977; Bartnicki, 1989). Finite elements with linear shape functions are applied to vertical advection. Diffusion is solved using a combination of the finite elements method and the θ-method (e.g. Morton and Mayers, 2005, Sect. 2.10). The chemistry solver involved a combination of a second-order, two-step, variable step-size backwards differentiation formula (Verwer et al., 1996) and the Euler backward iterative method (Hertel et al., 1993). Lateral boundary conditions are either free or fixed, depending on the wind direction at the boundaries – see Frohn et al. (2002) for further references and details.

2.3 Optimal interpolation

As mentioned above, the algorithm presented here is based on the two-dimensional OI DA scheme of Frydendall et al. (2009). The following describes version V2.0 of this scheme (cf., version V1.0, as presented by Frydendall et al., 2009).

The assimilation was performed once an hour, if any retrievals were available in the model domain in the previous hour. No special treatment was used to account for the time discrepancy between the model and OMI data, due to short interval between assimilation cycles.

GMDD
5, 309–346, 2012

For simpler comparison between the observed and modelled fields, we calculated the two-dimensional tropospheric NO_2 column concentrations based on the modelled three-dimensional NO_2 concentrations. This was done by summing the mass of NO_2 at each model level up to a height of 9 km, approximately the height of the tropopause in the higher latitudes. Thus the background is a two-dimensional field. After the assimilation, at each point in the two-dimensional field the mass of NO_2 was redistributed over vertical levels up to 9 km such that the proportions of mass at each level were unaltered.

We now summarise the OI DA scheme of Frydendall et al. (2009), which was used to assimilate O_3 observations. Let $\boldsymbol{x}_\mathrm{b}$ and $\boldsymbol{y}_\mathrm{o}$ be vectors of the background (in this case, the modelled tropospheric NO_2 column concentrations) and observed variables (in this case, OMI estimates of tropospheric NO_2), respectively. Let $\mathbf{B}$ and $\mathbf{R}$ be the error covariance matrices for $\boldsymbol{x}_\mathrm{b}$ and $\boldsymbol{y}_\mathrm{o}$ respectively. Let $\mathbf{H}$ be the linear transformation from the model space to the observation space. Then the analysed field $\boldsymbol{x}_\mathrm{a}$ is estimated (Kalnay, 2003, pages 150–156) by

$$\boldsymbol{x}_\mathrm{a} = \boldsymbol{x}_\mathrm{b} + \mathbf{B}\mathbf{H}^T \left(\mathbf{H}\mathbf{B}\mathbf{H}^T + \mathbf{R}\right)^{-1} (\boldsymbol{y}_\mathrm{o} - \mathbf{H}\boldsymbol{x}_\mathrm{b}). \quad (1)$$

The background error covariance matrix is parameterised using the correlation function of Balgovind et al. (1983),

$$f(r; e_\mathrm{b}, L) = e_\mathrm{b}(1 + r/L)e^{-r/L} \quad (2)$$

where r is the horizontal distance between two points, e_b is the background error weight, and L is the correlation length scale. Only horizontal distances were considered since the background field was two-dimensional. The entries of $\mathbf{B}$, the background error covariance matrix, are given by

$$\mathbf{B}_{ij} = \frac{1}{2}\left(f(r_{ij}; e_\mathrm{b}, \tilde{L}_i) + f(r_{ij}; e_\mathrm{b}, \tilde{L}_j)\right)$$

where r_{ij} is the horizontal distance between the i-th and j-th model variables, and $\tilde{L}_i$ is the adjusted correlation length scale accounting for the number of observations in the

GMDD
5, 309–346, 2012

neighborhood of the i-th variable. The adjustment, suggested by Hoelzemann et al. (2001), is:

$$\tilde{L}_i = (1 - \min(\delta_i, 8)/10)L \quad (3)$$

where δ_i is the number of observations within distance L of the i-th variable, for characteristic length scale L. The linear observation operator, $\mathbf{H}$, was composed of a bi-linear interpolation to the locations of the four grid points surrounding each observation.

2.4 Parameter estimation

Frydendall et al. (2009) estimated the weight of the background, relative to the observation, e_b, and the correlation length scale, L, based on innovation statistics (Hollingsworth and Lonnberg, 1986). This involves plotting the correlations of the innovations (i.e. $\boldsymbol{y}_o - \mathbf{H}\boldsymbol{x}_b$) as a function of the distance between observations, and fitting Eq. (2) to this scatter-plot (Fig. 2).

If observations are obtained at fixed locations and at synchronised time-points, the correlation between a pair of locations is calculated by a pairwise comparison of the time-series of innovations. This is *not* possible for satellite data, as there is only one monitoring instrument and observations are both asynchronous and occur at different locations.

A substitute for time-series at fixed locations was created using a binning strategy, as described below:

1. Ignore OMI data from the outermost 4 rows and columns of the DEHM's 96×96 grid, thus providing a buffer for potential boundary effects.
2. For each satellite retrieval inside this 88×88 grid, extract from the model the corresponding value by bi-linear interpolation to the middle of corresponding OMI pixel
3. Calculate the innovation (i.e. observed – predicted), and associate it with the nearest model grid-point, thereby binning the innovations.

GMDD
5, 309–346, 2012

4. Repeat steps 2–3, recording at most one innovation per bin per hour (since this was the frequency of the DA step).

5. For each pair of bins, calculate the correlation between innovations at the two grid-points for only those time-points when innovations were available in both bins at the same hour of the same day.

6. Plot the correlations calculated in step 5. against the distance between the grid-points (Fig. 2).

Equation (2) was fitted to these data by minimising the objective function

$$g = \sum_{k=1}^{K} \frac{m_k}{r_k^2} (c_k - f(r_k; e_b, L))^2 \quad (4)$$

where m_k is the number of points used to calculate the k-th correlation c_k – in other words, m_k is the number of synchronous observations in the k-th pair of bins. Furthermore r_k is the distance between the k-th pair of bins, and K is the total number of pairs of bins with a sufficient number of synchronous observations ($m_k \geq 5$) to calculate a correlation. Thus pairs of bins close together and with many synchronous observations were given the most weight, in order to better estimate the intercept parameter, e_b. The PORT optimization library (Gay, 1990) was used to minimise Eq. (4).

The resulting parameter estimates were $L = 212$ km and $e_b = 0.45$ for the NO_2 satellite retrievals, compared with $L = 270$ km and $e_b = 0.86$ as calculated by Frydendall et al. (2009) for the ground-based O_3 data.

3 Experiments and verification

3.1 Data assimilation experiments

Frydendall et al. (2009) examined several configurations of their OI scheme to assimilate in situ O_3 measurements. There are important differences compared to this study:

GMDD
5, 309–346, 2012

we are assimilating satellite retrievals of tropospheric NO_2, and using a different and more advanced CTM. Thus we assume that the optimal configuration in the present situation will differ from that of Frydendall et al. (2009). In this section, we describe the DA experiments performed in order to find a good configuration for the OI solver in this context (see Table 1 for a summary).

Experiment *ref* involved no DA, and thus represents a "baseline" for the other experiments. Experiment *1* used the same configuration as the best-performing experiment from Frydendall et al. (experiment 8 in that article). In all other experiments, the background error covariance matrix was parameterised using the correlation length and background error weight estimated with the OMI retrievals ($L = 212$ km, and $e_b = 0.45$).

The spatial density of observations assimilated was much higher in this study than in Frydendall et al. (2009). We considered different methods of down-weighting observations in regions of high observational density in the background error covariance matrix – this involved different forms of Eq. (3). When we consider the number of observations within a distance of $L = 212$ km from each grid-point, the 70 % quantile of this distribution was 75 observations, and thus the parameters for Eq. (3) were adjusted to reflect this in experiment *3*:

$$\tilde{L}_i = (1 - \min(\delta_i, 75)/100)L$$

As mentioned in Sect. 2.1, an estimate of the uncertainty of the retrieved NO_2 concentration was provided by the retrieval process. This was used to parameterise the observation error covariance matrix in experiment *4*, by setting $\mathbf{R}_{ii}$, the error estimate of observation i, to the corresponding uncertainty estimate, σ_i. We note that both the retrieved value and associated error measurement were typically in the order of 10^{15} molecules NO_2 per cm^2, and so we scaled observation errors by a factor of 10^{-15}.

There was, however, a strong, positive correlation between the observations and the associated uncertainty estimates ($R^2 = 0.95$). Thus, in experiment *5*, we considered whether the *relative* uncertainty of observations (i.e. $y_{o,i}/\sigma_i$) was a more meaningful way of parameterising the observation error covariance matrix. The rationale was that

GMDD
5, 309–346, 2012

the absolute uncertainty would consistently down-weight large observations (due to the correlated noted above), potentially leading to bias.

3.2 Verification with EMEP data

Observations of NO_2 and O_3 concentrations for the year 2005 were obtained from ground-based measuring stations from the EMEP network (Aas, 2008). Time series of daily average concentrations were available at 38 stations recording NO_2, and 121 stations recording O_3 (Fig. 1). The different experiments were assessed by comparing the analysed fields to these measurements.

The DEHM describes a total of 63 atmospheric components, however we examine results for only two: NO_2 and O_3. Our main interest is in how the accuracy of NO_2 estimates varies when assimilating this species. We also chose to examine O_3, as it has a close chemical relationship with NO_2 and has important consequences for human health.

For each day, the (spatial) average over all stations was calculated for the observed and calculated concentrations (Fig. 3). Based on the observed and calculated time-series, we computed the correlation coefficient (R^2), the normalised mean squared error (NMSE) and the fractional bias (FB) – see Brandt et al. (1998) for definitions. Results are shown in Table 2.

3.3 Comparison with OMI retrievals

To compare the different DA experiments, we also examined how well the predicted NO_2 tropospheric concentration fields matched the satellite retrievals. For the satellite data, OMI observations were binned to the same 96×96 grid as the calculated values, and daily averages were calculated for each bin. The annual average for the OMI data was calculated from these daily averages.

Similarly, for the modelled data, annual averages were calculated from daily averages. The daily averages were calculated as the mean concentration over the period

GMDD
5, 309–346, 2012

10:00 to 14:00 GMT, which corresponds to the interval containing most of the satellite overpasses. One complication was that in the binned OMI daily averages, only a fraction of bins contained observations (in the example shown in Fig. 4, grid-cells with no data are represented as grey squares). For a fair comparison of the OMI and modelled data, this pattern of "missing data" was therefore replicated when calculating the annual average of modelled values. Seasonal averages were calculated similarly, but restricted to the periods April–September and January–March/October–December, which are henceforth referred to as "AMJJAS" and "JFM-OND", respectively. The resulting fields are shown in Figs. 5 and 6.

The observed and modelled annual mean tropospheric NO_2 fields are compared on the basis of the R^2, NMSE and FB (see Table 3).

3.4 Comparison with ozonosondes

The vertical profile of O_3 concentrations has an important influence on the radiation balance of the troposphere and stratosphere (Jacob, 1999). Given the strong relationship between O_3 and NO_2, we compared modelled O_3 profiles with those measured by ozonosondes; these data were made available by the Network for the Detection of Atmospheric Composition Change (NDACC, www.ndsc.ncep.noaa.gov). Observed O_3 profiles were interpolated to the heights of the model layers using cubic splines; seasonal averages were calculated for AMJJAS and JFM-OND from the interpolated profiles. We present results from two measurement sites: De Bilt (Holland) and Legionowo (Poland); see Fig. 7.

There are several different definitions for the tropopause (the boundary between the stratosphere and the troposphere); while it is typically defined based on lapse rate, the tropopause height can also be calculated based on the gradient of O_3 profile. The thermal and O_3 definitions usually agree reasonably well, although the O_3 tropopause is typically about 800 m below the thermal tropopause (Bethan et al., 1996). The points marked on Fig. 7 show the O_3 tropopause height, using the definition of Bethan et al. (1996).

GMDD
5, 309–346, 2012

3.5 Perturbation of initial conditions

Data assimilation is typically used to optimize initial conditions. For CTMs, the influence of initial conditions typically decays as the simulation proceeds. Thus the potential effectiveness for improving air quality forecasts is limited by how rapidly a perturbation to the initial conditions dissipates. To investigate how long the perturbation of the NO_2 field lasts, we ran two different simulations. These were initialised by concentration fields generated by experiments *ref* and *3*. They were run for the period 1 July 2005 to 31 July 2005. We then calculated, for each hour, the mean ground-level concentration averaged over the entire domain and the root mean squared difference between the two simulations for both O_3 and NO_2 (see Fig. 8).

4 Results

4.1 EMEP

Table 2 presents the verification statistics for the 5 experiments. Experiments *1–5* were more successful than *ref* at estimating NO_2 concentrations, with experiments *2* and *3* giving the best results. The situation is not so simple for the O_3 results (see also Fig. 3), where experiment *ref* showed a higher NMSE and bias, but also higher R^2 than most of the other experiments. Among the experiments using DA, experiment *5* had the lowest bias and the highest R^2 value for O_3, but was less effective at estimating NO_2. The results for O_3 for experiments *2–5* showed a common pattern for O_3 of lower NMSE and FB, but also marginally lower R^2 compared to experiment *ref*.

Figure 3 shows the time-series of daily means, averaged over available measurement stations. We see that NO_2 concentrations (both modelled and measured) are higher and more variable during the period JFM-OND compared to during the period AMJJAS. The greatest changes, due to the use of DA, in the modelled NO_2 time-series are observed during JFM-OND. Without DA, the model underestimates NO_2 concentrations and does not capture the amplitude of temporal variability.

GMDD
5, 309–346, 2012

Changes, due to the use of DA, in the modelled O_3 time-series are less dramatic as for NO_2. Experiment *ref* tended to slightly overestimate O_3 concentrations in the second half of the year, whereas experiments *2–5* appear to be less biased during this period. Otherwise, the shape of the modelled O_3 time-series was fairly similar between experiments.

4.2 OMI

We compared modelled and measured fields of annual mean tropospheric NO_2 concentrations (Table 3). We see that even without DA (experiment *ref*), the estimates from the DEHM of tropospheric NO_2 describe a large proportion of spatial variability observed in the corresponding OMI field ($R^2 = 0.923$). Experiments *2* and *3* had the lowest NMSE and bias. Experiments *1–5* show very similar correlations to the observed OMI field.

Consistent with the higher NO_2 concentrations seen in the time-series, Fig. 5 shows that the use of DA led to an increase in NO_2 that was widely spread across the model domain. The clearest changes are seen in eastern Europe and western Russia. The time-series also suggested important seasonal effects, and Fig. 6 presents the seasonally averaged mean tropospheric column concentrations across the model domain. The differences between experiments *ref* and *3* show, generally speaking, the same patterns as were observed for the annual average. However over the Po valley in northern Italy there is a stronger adjustment during the months JFM-OND than during the months AMJJAS.

4.3 Ozonosondes

Figure 7 shows the comparison between seasonally averaged modelled and measured O_3 profiles at two locations, from ground level up to around 14 km altitude. There is satisfactory agreement between the observed and modelled profiles.

GMDD
5, 309–346, 2012

Up to around 8000 m, the O_3 mixing ratio increase slowly with height, and above this it grows rapidly. The modelled O_3 tropopause appears to be higher in the period AMJJAS compared with JFM-OND, which is consistent with other studies of seasonal patterns of the thermal tropopause (Hall et al., 2011). This was not clearly reflected in the observed ozonosonde profiles, however this appears to be due to the effects of the interpolation of the observed profile to the heights of the model levels.

We see that the O_3 concentrations from experiment *3* (using DA) was a few ppb lower than for experiment *ref* (without DA), and this difference was reasonably consistent across sites, seasons and altitudes. The shift in the O_3 profiles appears to be due to the way in which the NO_2 profile was altered: the assimilation scheme preserved the shape of the NO_2 profile, adjusting only the total mass of the column.

4.4 Perturbation duration

We compared two simulations that were identical except for their initial conditions: they were initialised using concentration fields from experiments *ref* and *3*, respectively. Neither of these two simulations used DA. Figure 8 shows that for NO_2 the differences between the two simulations decay over 2–3 days, whereas for O_3 a comparable convergence takes place in the order of 5–10 days. This is largely a reflection of the difference in atmospheric lifetime of these species at the surface.

5 Discussion

The assimilation of NO_2 led to a reduced bias for O_3 (note that, without DA, this bias was already quite low), however it also resulted in a slight decrease in the correlation between the observed and modelled surface O_3. We expect that this decrease in correlation is due to the spread of information from cloud-free regions to cloudy regions. Retrieved NO_2 concentrations were not assimilated if the pixel appeared to contain even small amounts of cloud. However cloud cover affects tropospheric chemistry in several ways (e.g. radiation balance, wet deposition), and this information spread from cloud-free to cloudy regions may degrade the accuracy of the modelled concentration

GMDD
5, 309–346, 2012

field in some regions.

The year-long span of the simulations allowed us to consider seasonal variation. For example, the use of DA improved the modelled NO_2 concentrations in the winter particularly, when concentrations are higher and more variable. Also, the adjustment to concentrations in the Po Valley (Italy) was much stronger during the winter months, suggesting that features in, for example, the emissions or meteorology in this region was less well represented during the winter months.

Our choice to adjust the NO_2 profile while keeping the profile shape constant has an underlying assumption that the modelled profile is reasonably accurate. Although vertical profiles of NO_2 are not measured routinely, ozonosonde data were used for validation. Given the close relationship between the two species, this can be considered a "proxy" for validation of the NO_2. The vertical O_3 profiles indicated good agreement with measurements and showed a small but relatively consistent shift due to the effect of assimilating NO_2. The simulations which used DA showed slightly lower average O_3 concentrations.

The increased NO_2 concentrations induced by the assimilation of OMI retrievals most likely corrects for a bias in the emission rates used (potentially both in the total annual emission per grid-cell and also its temporal distribution) by the DEHM. If so, then the assimilation becomes a "source" of NO_2, and biases in the emission rates are not addressed directly.

In this study, we estimated the background weight as $e_b = 0.45$, compared to $e_b = 0.86$ as calculated by Frydendall et al. (2009). The lower background weight indicates a lower correlation between the OMI retrieved tropospheric NO_2 column concentrations and the modelled values from the DEHM. At an hourly resolution, the correspondence between the OMI and DEHM fields is not as strong as for the for annual averages (see Fig. 5 and Table 3). This may suggest that there is greater noise in the OMI data (compared to surface O_3 measurements) or that the model required substantially more correction compared to the ground-level O_3 concentrations from the DEOM, used by Frydendall et al. (2009). Furthermore, the decorrelation length scale found here

GMDD
5, 309–346, 2012

($L = 212$ km) is shorter than the value $L = 270$ km that used by Frydendall et al. (2009), reflecting the shorter atmospheric lifetime of NO_2 compared to O_3 and the more "local" nature of NO_2.

In a similar study, Wang et al. (2011) used an OI scheme to assimilate retrievals of tropospheric NO_2 retrievals from OMI into the CTM Polyphemus (Mallet et al., 2007). The NO_2 column concentrations were adjusted in the same manner as was done in this study (namely, the modelled profile was scaled and the profile shape was kept constant). Wang et al. (2011) used a very similar parameterisation of the background covariance matrix, **B**. Rather than estimating the relevant parameters using innovation statistics, they ran a series of simulations with different values of the parameters, and chose the parameter values which gave the lowest RMSE compared with EMEP in situ measurements. They found an optimal values of $L = 3^\circ$ latitude/longitude; while this is not immediately comparable to kilometer distances, since distance between neighbouring latitude/longitude grid-points depend on latitude, a 3° difference in longitude corresponds to a distance 214 km at 50° latitude. Furthermore, Wang et al. (2011) estimate the background weight as $e_b = 0.71$ (which is the reciprocal of their parameter $A = R/B$, the ratio of the background and observation errors), which places greater weight on modelled values than was done in this study.

Wang et al. (2011) evaluated both the analysis and the day-ahead forecasts, and showed that there was a slight improvement in the forecast (reference RMSE = 5.8 $\mu g\,m^{-3}$, analysis RMSE = 4.9 $\mu g\,m^{-3}$, forecast RMSE = 5.4 $\mu g\,m^{-3}$). As shown here, the effect of differences in the initial conditions for NO_2 can be seen for at least 1–2 days.

This study complements that of Wang et al. (2011) in a number of ways. The simulation period of one year allowed us to consider seasonal effects, which were not fully accounted for in the simulations of Wang et al. (2011), which spanned three months. Furthermore, we considered not only the resulting NO_2 concentrations but also the indirect effects to O_3 due to assimilating NO_2. Finally, we detail a different method of estimating parameters defining the background covariance matrix.

GMDD
5, 309–346, 2012

The OI assimilation scheme is both conceptually simple and straightforward to implement. If both the length of control vector (i.e. those modelled variables that the DA adjusts) and the number of observations are sufficiently small, then it may be less computationally demanding than other assimilation schemes. However the OI framework described here is, in several ways, rather limited. Firstly, during the assimilation, we updated only a two-dimensional field for a single component (roughly 10^4 variables). This procedure cannot be scaled to handle simultaneously all modelled components at all vertical layers (roughly 10^7 variables) without making further simplifications, which may well degrade the scheme's performance (Kalnay, 2003, chapter 5). Secondly, the innovation statistics method for estimating parameters of the background covariance matrix requires large amounts of measurement data, and the derived statistics are only representative for the regions where the data are available; most air quality measurement networks are sparse and unevenly distributed geographically. Thirdly, the method does not scale well as the number of observations increases, since to compute the Kalman gain matrix, it is necessary to solve a system of equations with dimension equal to the number of observations. Far more flexible approaches to chemical DA are offered by variational or Kalman filter-based schemes (see Lahoz et al., 2007, and references therein).

For historical re-analysis or for single-component, single-layer assimilation, then it is possible that OI is a sufficiently competent scheme, beyond which any gains are marginal and require a significantly more complicated and computationally demanding DA procedure (Wu et al., 2008). In a forecasting context, however, the strong forcings from chemistry and emissions entail that the effect of better initial conditions will decay during the forecast outlook, although the rate depends on the atmospheric lifetime of the species in question and whether they are emitted directly or formed by secondary reactions. The framework of DA can be used to re-estimate highly uncertain model parameters (e.g. emission rates, as were examined by Elbern et al., 2007), and this appears to be a promising means of addressing forecast accuracy for directly emitted, short-lived atmospheric components such as NO_2; however, this is beyond the scope

GMDD
5, 309–346, 2012

of OI.

The DA scheme described here could be developed in several ways. For example, the observations were originally provided as pixels, thereby corresponding to a two-dimensional region. However for simplicity they were summarised at the region's midpoint. A more accurate version of the observation operator would account for the fact that pixels may span multiple grid-cells.

Another potential adjustment would be a more adaptive parameterisation of the background covariance. Current estimates of the key parameters (e_b and L) are based on an entire year's worth of data. These parameters could potentially be estimated separately for each month, and separately for areas of high or low concentrations. This would need to be done off-line before they could be used operationally. This would help account, for example, for strong seasonal variation in NO_x lifetimes (Schaub et al., 2007).

However, instead of extending the OI scheme presented here, we are developing an ensemble Kalman filter assimilation system, which we expect will be more flexible and extensible than the OI framework.

6 Conclusions

In this study, we have presented a thorough description of an algorithm used to assimilate remotely-sensed tropospheric NO_2 column concentrations. We conducted a number of experiments to assess the performance of different configurations of the assimilation. Results were compared to observations from a number of independent data sets. The analysed concentration fields were substantially more accurate (when compared to measurements from regional background monitoring station) than those of the simulation without DA, with reduced bias for both NO_2 and O_3. The use of appropriately calculated parameters (the length-scale and background covariance weight) for the background covariance matrix also led to better results. Furthermore, appropriately chosen parameters to account for local observation density yielded a small improvement on top of this. The different parameterisation of the observation covariance error

GMDD
5, 309–346, 2012

matrix had little effect on the validation statistics. A slight decrease in the correlation between the observed and modelled surface O_3 may be due to the effects of excluding data from cloudy regions.

Despite its limitations, the optimal interpolation algorithm is conceptually simple and straightforward to implement, and proved it to be useful in this context. We have demonstrated that the effects of chemical DA are not limited to the assimilated species, and can be seen in chemically related compounds. Finally, the effectiveness of chemical DA in a forecasting context must be considered in conjuction with the atmospheric lifetime of the species in question.

Acknowledgements. We are grateful to the EMEP consortium for providing the ground-based observations, the NDACC for providing the ozonosonde data, the European space agency for providing the OMI retrievals, Zahari Zlatev (Aarhus University) for helpful discussions, and Thomas Becker (Aarhus University) for GIS support. This study was funded by the European Space Agency's PROMOTE project (www.gse-promote.org).

References

Aas, W. (Ed.): Data quality 2006, quality assurance, and field comparisons, EMEP/CCC-Report 3/2008, EMEP Co-operative Programme for Monitoring and Evaluation of the Long-range Transmission of Air Pollutants in Europe, Norwegian Institute for Air Research, Kjeller, Norway, www.emep.int, 2008. 321

Adhikary, B., Kulkarni, S., Dallura, A., Tang, Y., Chai, T., Leung, L. R., Qian, Y., Chung, C. E., Ramanathan, V., and Carmichael, G. R.: A regional scale chemical transport modeling of Asian aerosols with data assimilation of AOD observations using optimal interpolation technique, Atmos. Environ., 42, 8600–8615, 2008. 312

Balgovind, R., Dalcher, A., Ghil, M., and Kalnay, E.: A stochastic-dynamic model for the spatial structure of forecast error statistics, Mon. Weather Rev., 111, 701–722, 1983. 317

Bartnicki, J.: A simple filtering procedure for removing negative values from numerical solutions of the advection equation, Environ. Softw., 4, 187–201, 1989. 316

Belanger, K., Gent, J. F., Triche, E. W., Bracken, M. B., and Leaderer, B. P.: Association of In-

GMDD

5, 309–346, 2012

door Nitrogen Dioxide Exposure with Respiratory Symptoms in Children with Asthma, American Journal of Respiratory and Critical Care Medicine, 173, 297–303, 2006. 313
Benkovitz, C. M., Scholtz, M. T., Pacyna, J., Tarrasón, L., Dignon, J., Voldner, E. C., Spiro, P. A., Logan, J. A., and Graedel, T. E.: Global gridded inventories of anthropogenic emissions of sulfur and nitrogen, J. Geophys. Res., 101, 29239–29254, 1996. 316
Bethan, S., Vaughan, G., and Reid, S. J.: A comparison of ozone and thermal tropopause heights and the impact of tropopause definition on quantifying the ozone content of the troposphere, Q. J. Roy. Meteorol. Soc., 122, 929–944, 1996. 322, 345
Black, T. L.: The New NMC Mesoscale Eta Model: Description and Forecast Examples, Weather Forecast., 9, 265–284, 1994. 316
Boersma, F., Bucsela, E., Brinksma, E., and Gleason, J. F.: Chapter 2: NO_2, in: OMI algorithm theoretical basis document, OMI trace gas algorithms, edited by: Chance, K., vol. IV, NASA technical report, 2002. 314
Boersma, K. F., Eskes, H. J., Veefkind, J. P., Brinksma, E. J., van der A, R. J., Sneep, M., van den Oord, G. H. J., Levelt, P. F., Stammes, P., Gleason, J. F., and Bucsela, E. J.: Near-real time retrieval of tropospheric NO_2 from OMI, Atmos. Chem. Phys., 7, 2103–2118, doi:10.5194/acp-7-2103-2007, 2007. 314
Boersma, K., Jacob, D., Bucsela, E., Perring, A., Dirksen, R., van der A, R., Yantosca, R., Park, R., Wenig, M., Bertram, T., and Cohen, R.: Validation of OMI tropospheric NO_2 observations during INTEX-B and application to constrain NO_x emissions over the eastern United States and Mexico, Atmos. Environ., 42, 4480–4497, 2008. 313
Brandt, J., Bastrup-Birk, A., Christensen, J. H., Mikkelsen, T., Thykier-Nielsen, S., and Zlatev, Z.: Testing the importance of accurate meteorological input fields and parameterizations in atmospheric transport modelling, using DREAM – validation against ETEX-1, Atmos. Environ., 32, 4167–4186, 1998. 321
Brandt, J., Christensen, J. H., Frohn, L. M., and Berkowicz, R.: Operational air pollution forecasts from regional scale to urban street scale; Part 1: System description, Phys. Chem. Earth, B, 26, 781–786, 2001a. 314, 315
Brandt, J., Christensen, J. H., Frohn, L. M., and Berkowicz, R.: Operational air pollution forecasts from regional scale to urban street scale; Part 2: Performance evaluation, Phys. Chem. Earth, B, 26, 825–830, 2001b. 315
Brandt, J., Christensen, J. H., Frohn, L. M., Palmgren, F., Berkowicz, R., and Zlatev, Z.: Operational air pollution forecasts from European to local scale, Atmos. Environ., 35, 91–98,

GMDD
5, 309–346, 2012

2001c. 315
Carmichael, G. R., Sandu, A., Chai, T. F., Daescu, D. B., Constantinescu, E. M., and Tang, Y. H.: Predicting air quality: Improvements through advanced methods to integrate models and measurements, J. Comput. Phys., 227, 3540–3571, 2008. 311, 312
Christensen, J. H.: The Danish Eulerian hemispheric model – a three-dimensional air pollution model used for the arctic, Atmos. Environ., 31, 4169–4191, 1997. 315
Dardub, D. and Seinfeld, J. H.: Numerical advective schemes used in air quality models – sequential and parallel implementation, Atmos. Environ., 28, 3369–3385, 1994. 316
Elbern, H., Strunk, A., Schmidt, H., and Talagrand, O.: Emission rate and chemical state estimation by 4-dimensional variational inversion, Atmos. Chem. Phys., 7, 3749–3769, doi:10.5194/acp-7-3749-2007, 2007. 328
Forester, C. K.: Higher order monotonic convective difference schemes, J. Comput. Phys., 23, 1–22, 1977. 316
Frohn, L. M., Christensen, J. H., and Brandt, J.: Development of a high-resolution nested air pollution model, J. Comput. Phys., 179, 68–94, 2002. 315, 316
Frydendall, J., Brandt, J., and Christensen, J. H.: Implementation and testing of a simple data assimilation algorithm in the regional air pollution forecast model, DEOM, Atmos. Chem. Phys., 9, 5475–5488, doi:10.5194/acp-9-5475-2009, 2009. 314, 316, 317, 318, 319, 320, 326, 327
Gay, D. M.: Usage Summary for Selected Optimization Routines, Computing Science Technical Report 153, AT & T Bell Laboratories, 1990. 319
Hall, C. M., Hansen, G., Sigernes, F., and Kuyeng Ruiz, K. M.: Tropopause height at 78° N 16° E: average seasonal variation 2007–2010, Atmos. Chem. Phys., 11, 5485–5490, doi:10.5194/acp-11-5485-2011, 2011. 325
Hertel, O., Berkowicz, R., Christensen, J., and Hov, Ø.: Test of two numerical schemes for use in atmospheric transport-chemistry models, Atmos. Environ., 27A, 2591–2611, 1993. 316
Hoelzemann, J. J., Elbern, H., and Ebel, A.: PSAS and 4D-var Data Assimilation for Chemical State Analysis by Urban and Rural Observation Sites, Phys. Chem. Earth, B, 26, 807–881, 2001. 318
Hollingsworth, A. and Lonnberg, P.: The Statistical Structure of Short-Range Forecast Errors As Determined from Radiosonde Data. 1: the Wind-Field, Tellus A, 38, 111–136, 1986. 314, 318
Huijnen, V., Eskes, H. J., Poupkou, A., Elbern, H., Boersma, K. F., Foret, G., Sofiev, M.,

GMDD
5, 309–346, 2012

Valdebenito, A., Flemming, J., Stein, O., Gross, A., Robertson, L., D'Isidoro, M., Kioutsioukis, I., Friese, E., Amstrup, B., Bergstrom, R., Strunk, A., Vira, J., Zyryanov, D., Maurizi, A., Melas, D., Peuch, V.-H., and Zerefos, C.: Comparison of OMI NO_2 tropospheric columns with an ensemble of global and European regional air quality models, Atmos. Chem. Phys., 10, 3273–3296, doi:10.5194/acp-10-3273-2010, 2010. 313

Ionov, D., Goutail, F., Pommereau, J.-P., Bazureau, A., Kyro, E., Portafaix, T., Held, G., Ericksen, P., and Dorokhov, V.: Ten Years of NO_2 Comparisons Between Ground-Based SAOZ and Satellite Instruments (GOME, Sciamachy, OMI), in: Proceedings of Atmospheric Science Conference, edited by Lacoste, H. and Ouwehand, L., no. ESA SP-628 in European Space Agency, ESRIN, Frascati Italy, 2006. 313

Jacob, D.: Introduction to atmospheric chemistry, Princeton University Press, Princeton, NJ, USA, 1999. 312, 322

Jacobson, M. Z.: Fundamentals of atmospheric modelling, Cambridge University Press, Cambridge, UK., 2005. 311

Janjic, Z. I.: The step-mountain coordinate: Physical package, Mon. Weather Rev., 118, 1429–1443, 1990. 316

Janjic, Z. I.: The step-mountain Eta coordinate model: Further developments of the convection, viscous sublayer, and turbulence closure schemes, Mon. Weather Rev., 122, 927–945, 1994. 316

Kalnay, E.: Atmospheric modelling, data assimilation and predictability, Cambridge University Press, Cambridge, United Kingdom, 2003. 311, 312, 317, 328

Kemp, K., Ellermann, T., Brandt, J., Christensen, J., Ketzel, M., and Jensen, S. S.: The Danish Air Quality Monitoring Programme: Annual Summary for 2007, NERI Technical Report No. 681, National Environmental Research Institute, Aarhus University, Denmark, http://www2.dmu.dk/Pub/FR681.pdf, 2008. 315

Lahoz, W. A., Errera, Q., Swinbank, R., and Fonteyn, D.: Data assimilation of stratospheric constituents: a review, Atmos. Chem. Phys., 7, 5745–5773, doi:10.5194/acp-7-5745-2007, 2007. 328

Lamsal, L. N., Martin, R. V., van Donkelaar, A., Steinbacher, M., Celarier, E. A., Bucsela, E., Dunlea, E. J., and Pinto, J. P.: Ground-level nitrogen dioxide concentrations inferred from the satellite-borne Ozone Monitoring Instrument, J. Geophys. Res., 113, D16308, doi:10.1029/2007JD009235, 2008. 313

Lanser, D. and Verwer, J.: Analysis of operator splitting for advection-diffusion-reaction prob-

GMDD

5, 309–346, 2012

lems from air pollution modelling, Journal of Computational and Applied Mathematics, 111, 201–216, 1999. 316
Mallet, V., Quélo, D., Sportisse, B., Ahmed de Biasi, M., Debry, É., Korsakissok, I., Wu, L., Roustan, Y., Sartelet, K., Tombette, M., and Foudhil, H.: Technical Note: The air quality modeling system Polyphemus, Atmos. Chem. Phys., 7, 5479–5487, doi:10.5194/acp-7-5479-2007, 2007. 327
Martin, R. V.: Satellite remote sensing of surface air quality, Atmos. Environ., 42, 7823–7843, 2008. 311
Matsui, T., Kreidenweis, S. M., Pielke Sr., R. A., Schichtel, B., Yu, H., Chin, M., Chu, D. A., and Niyogi, D.: Regional comparison and assimilation of GOCART and MODIS aerosol optical depth across the eastern U.S., Geophys. Res. Lett., 31, L21101, doi:10.1029/2004GL021017, 2004. 312
Mok, K. M., Miranda, A. I., Leong, K. U., and Borrego, C.: A Gaussian puff model with optimal interpolation for air pollution modelling assessment, Int. J. Environ. Pollut., 35, 111–137, 2008. 312
Morton, K. W. and Mayers, D. F.: Numerical solution of partial differential equations, Cambridge University Press, second edn., 2005. 316
Olivier, J. G. J. and Berdowski, J. J. M.: Global emissions sources and sinks, in: The Climate System, edited by Berdowski, J., Guicherit, R., and Heij, B. J., 33–78, A. A. Balkema Publishers/Swets & Zeitlinger Publishers, Lisse, The Netherlands, 2001. 316
Peters, J. M., Avol, E., Gauderman, W. J., Linn, W. S., Navidi, W., London, S. J., Margolis, H., Rappaport, E., Vora Jr., H., H. G., and Thomas, D. C.: A Study of Twelve Southern California Communities with Differing Levels and Types of Air Pollution II. Effects on Pulmonary Function, American Journal of Respiratory and Critical Care Medicine, 159, 768–775, 1999. 313
Pope, C. A.: Epidemiological Basis for Particulate Air Pollution Health Standards, Aerosol Sci. Technol., 32, 4–14, 2000. 313
Schaub, D., Brunner, D., Boersma, K. F., Keller, J., Folini, D., Buchmann, B., Berresheim, H., and Staehelin, J.: SCIAMACHY tropospheric NO_2 over Switzerland: estimates of NO_x lifetimes and impact of the complex Alpine topography on the retrieval, Atmos. Chem. Phys., 7, 5971–5987, doi:10.5194/acp-7-5971-2007, 2007. 313, 329
Schultz, M., Rast, S., van het Bolscher, M., Pulles, T., Brand, R., Pereira, J., Mota, B., Spessa, A., Dalsøren, S., van Nojie, T., and Szopa, S.: Emission data sets and methodologies for

GMDD
5, 309–346, 2012

estimating emissions, RETRO project report D1-6, 2007. 316
Searl, A.: A review of the acute and long term impacts of exposure to nitrogen dioxide in the United Kingdom, Research Report TM/04/03, Institute of Occupational Medicine, Edinburgh, United Kingdon, 2004. 313
Seinfeld, J. H. and Pandis, S. N.: Atmospheric chemistry and physics: from air pollution to climate change, Wiley, second edn., 2006. 312, 313
Simpson, D., Fagerli, H., Jonson, J. E., Tsyro, S., Wind, P., and Tuovinen, J.-P.: The EMEP Unified Eulerian Model. Model Description, EMEP MSC-W Technical Report 1/2003, Norwegian Meteorological Institute, Oslo, Norway, 2003. 316
Stieb, D. M., Judek, S., and Burnett, R. T.: Meta-Analysis of Time-Series Studies of Air Pollution and Mortality: Effects of Gases and Particles and the Influence of Cause of Death, Age, and Season, J. Air Waste Manage. Assoc., 52, 470–484, 2002. 313
Verwer, J. G., Blom, J. G., van Loon, M., and Spee, E. J.: A comparison of stiff ODE solvers for atmospheric chemistry problems, Atmos. Environ., 30, 49–58, 1996. 316
Vestreng, V. and Klein, H.: Emission data reported to UNECE/EMEP: Quality assurance and trend analysis & Presentation of WebDab, Msc-w status report, Norwegian Meteorological Institute, Oslo Norway, 2002. 316
Wang, X., Mallet, V., Berroir, J.-P., and Herlin, I.: Assimilation of OMI NO2 retrievals into a regional chemistry-transport model for improving air quality forecasts over Europe, Atmos. Environ., 45, 485–492, 2011. 313, 327
Wang, Y., McElroy, M. B., Boersma, K. F., Eskes, H. J., and Veefkind, J. P.: Traffic restrictions associated with the Sino-African summit: Reductions of NO_x detected from space , Geophys. Res. Lett., 34, L08814, doi:10.1029/2007GL029326, 2007. 313
WHO: Health Aspects of Air Pollution with Particulate Matter, Ozone and Nitrogen Dioxide, Tech. rep., World Health Organization, Bonn, Germany, report on a WHO Working Group, 2003. 313
Wu, L., Mallet, V., Bocquet, M., and Sportisse, B.: A comparison study of data assimilation algorithms for ozone forecasts, J. Geophys. Res., 113, D20310, doi:10.1029/2008JD009991, 2008. 312, 328
Zhao, C. and Wang, Y.: Assimilated inversion of NO_x emissions over east Asia using OMI NO_2 column measurements, Geophys. Res. Lett., 36, L06805, doi:10.1029/2008GL037123, 2009. 313

GMDD
5, 309–346, 2012

Table 1. A summary of the differences between the experiments. Abbreviations used: DA – whether data assimilation was applied, L – length scale parameter used in calculating the background covariance, e_b – background error weight, $\tilde{L}$ – length scale adjustment equation, $\mathbf{R}_{ii}$ – error estimate for the i-th observation, σ_i – uncertainty estimate (obtained from the retrieval procedure) associated with the i-th observation, δ – number of observations within distance L of a grid-point.

Experiment	DA	L (km)	e_b	$\tilde{L}$	$\mathbf{R}_{ii}$
ref	No	–	–	–	–
1	Yes	270	0.86	$(1-\max(\delta,8)/10)/L$	1
2	Yes	212	0.45	$(1-\max(\delta,8)/10)/L$	1
3	Yes	212	0.45	$(1-\max(\delta,75)/100)/L$	1
4	Yes	212	0.45	$(1-\max(\delta,8)/10)/L$	σ_i
5	Yes	212	0.45	$(1-\max(\delta,8)/10)/L$	σ_i/v_i

GMDD
5, 309–346, 2012

Table 2. Verification statistics calculated for each experiment based on ground-level concentrations at European monitoring stations. In each row, the two time series (shown in Fig. 3) compared are the mean observed and calculated concentrations, averaged over stations. For a summary of the different experiments, see Table 1. Abbreviations used: FB – fractional bias, NMSE – normalised mean squared error, R^2 – Pearson correlation coefficient.

	NO_2			O_3		
Exp	FB	NMSE	R^2	FB	NMSE	R^2
ref	−0.381	0.259	0.666	0.153	0.039	0.800
1	−0.352	0.219	0.722	0.178	0.052	0.781
2	−0.299	0.170	0.745	0.074	0.030	0.785
3	−0.302	0.170	0.758	0.071	0.029	0.788
4	−0.328	0.198	0.731	0.070	0.028	0.790
5	−0.326	0.194	0.731	0.054	0.024	0.799

GMDD
5, 309–346, 2012

Table 3. Verification statistics based on annual mean NO_2 tropospheric column concentrations. Each row represents a comparison (for a given experiment) of the annual mean tropospheric column concentration (e.g. the top panels of Fig. 5) against the mean retrieved concentration from OMI (see the bottom panel of Fig. 5); all grid-points in the domain are used in the comparison. See Table 2 for abbreviations used.

Experiment	FB	NMSE	R^2
ref	−0.381	0.385	0.923
1	−0.223	0.158	0.957
2	−0.122	0.110	0.952
3	−0.138	0.112	0.955
4	−0.193	0.166	0.946
5	−0.241	0.176	0.950

GMDD
5, 309–346, 2012

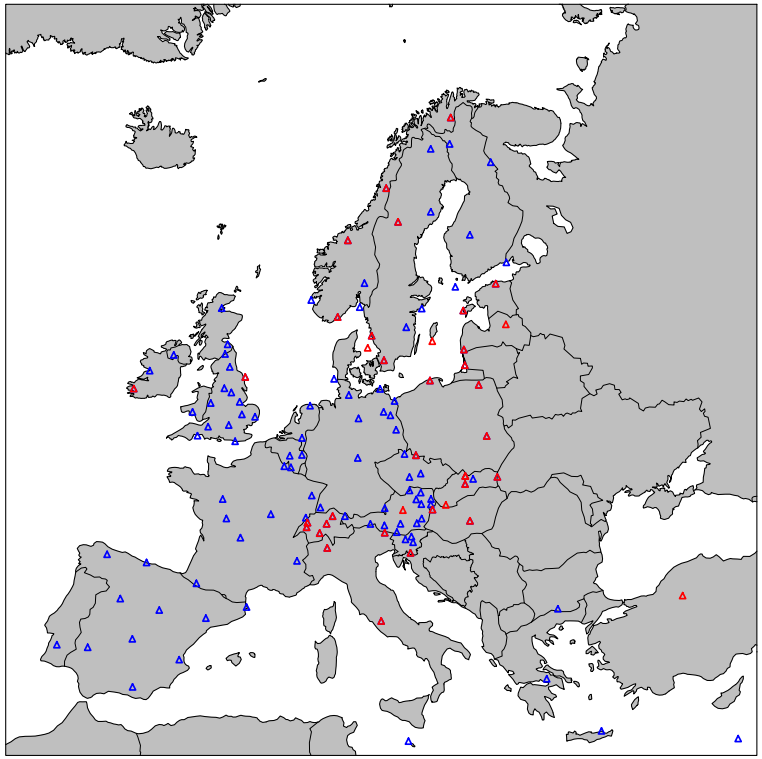

Fig. 1. Model domain used in this study. Locations of the EMEP monitoring stations for NO_2 and O_3 are shown in red and blue, respectively.

GMDD
5, 309–346, 2012

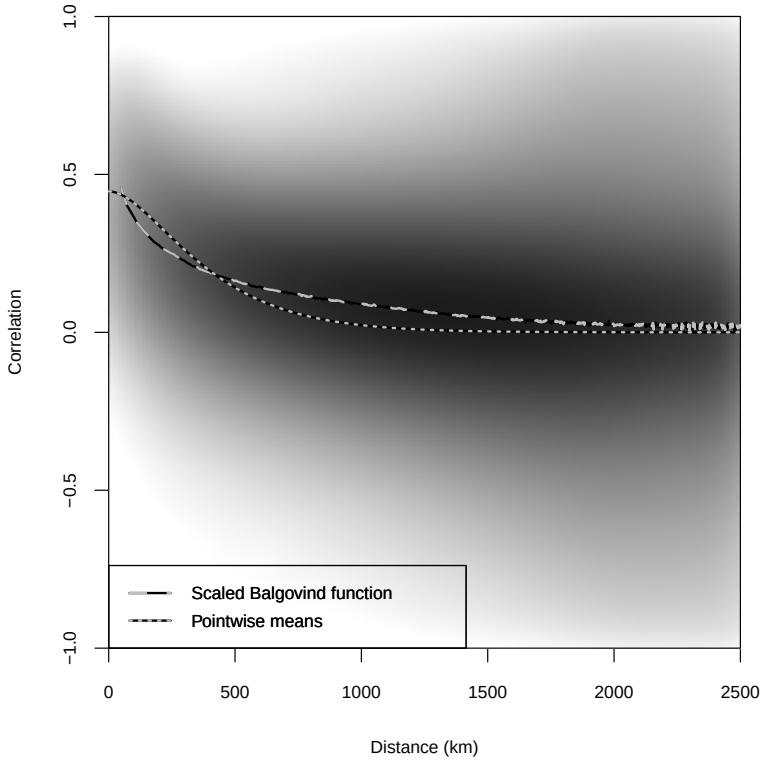

Fig. 2. Correlation between error innovations as a function as distance between grid-points. The correlation function $f(r) = e_b(1 + r/L)e^{-r/L}$ is shown with the dashed line, and the mean correlation at each distance is plotted with a dotted line. The 20 million points are summarised as a two-dimensional density plot.

GMDD
5, 309–346, 2012

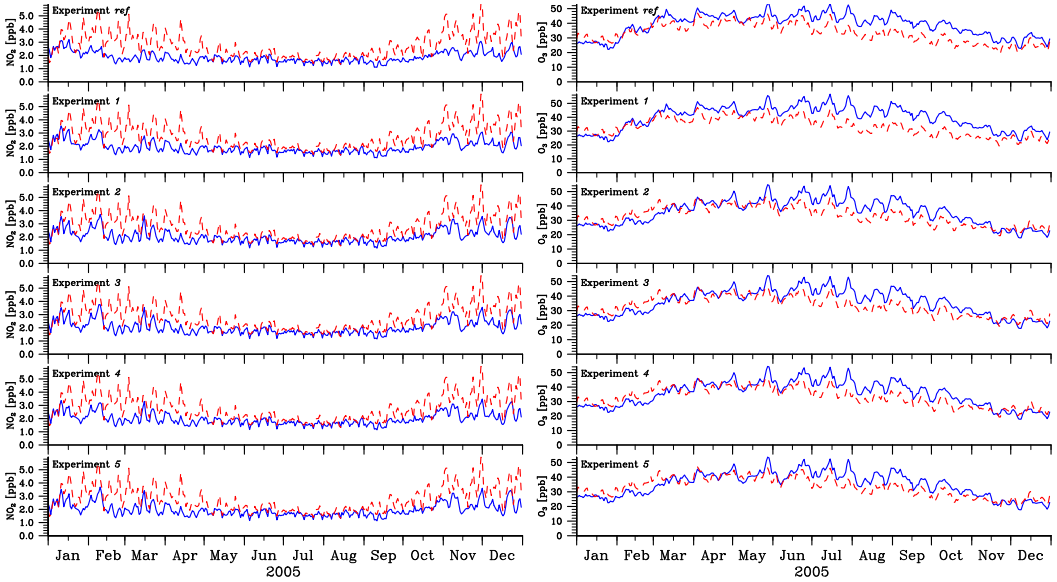

Fig. 3. Time-series of daily means of calculated (solid blue lines) and observed (dashed red lines) surface concentrations of NO_2 (left panel) and O_3 (right panel). For each day, the data were averaged (spatially) over available ground-based measurement stations, the locations of which are shown in Fig. 1. Verification statistics for these time-series are given in Table 2.

GMDD
5, 309–346, 2012

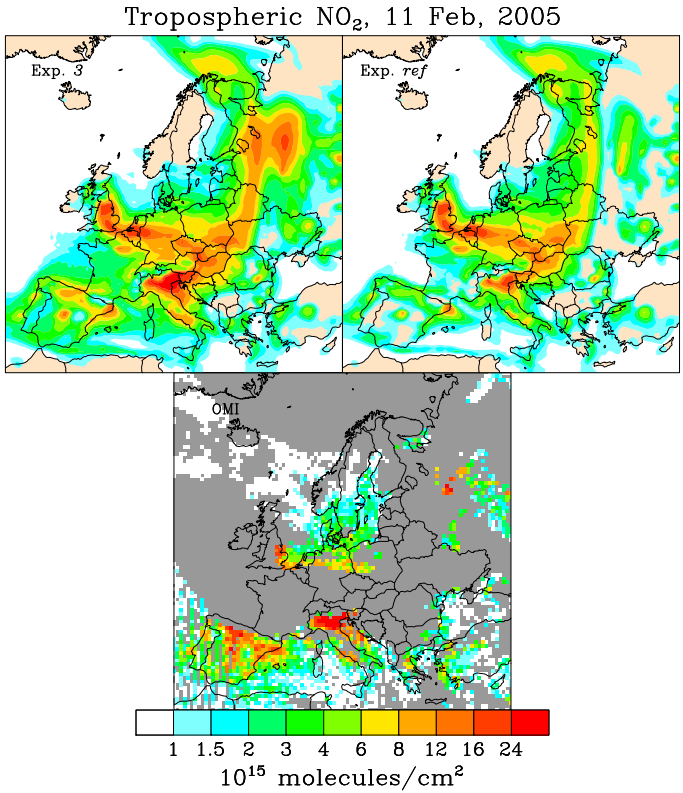

Fig. 4. Tropospheric NO_2 column concentrations for experiments *ref* and *3* (top) are compared to OMI retrievals (bottom) for a single day. Grey grid-cells represent bins containing no OMI data. As in Sect. 3.3, modelled values were averaged over the period 10:00 to 14:00, OMI data were binned to the same 96×96 grid as the modelled values, and daily averages were calculated for each bin. The OMI data are shown in raster (i.e. unsmoothed) format due to the high frequency of "missing data" (i.e. no observations within a bin).

GMDD
5, 309–346, 2012

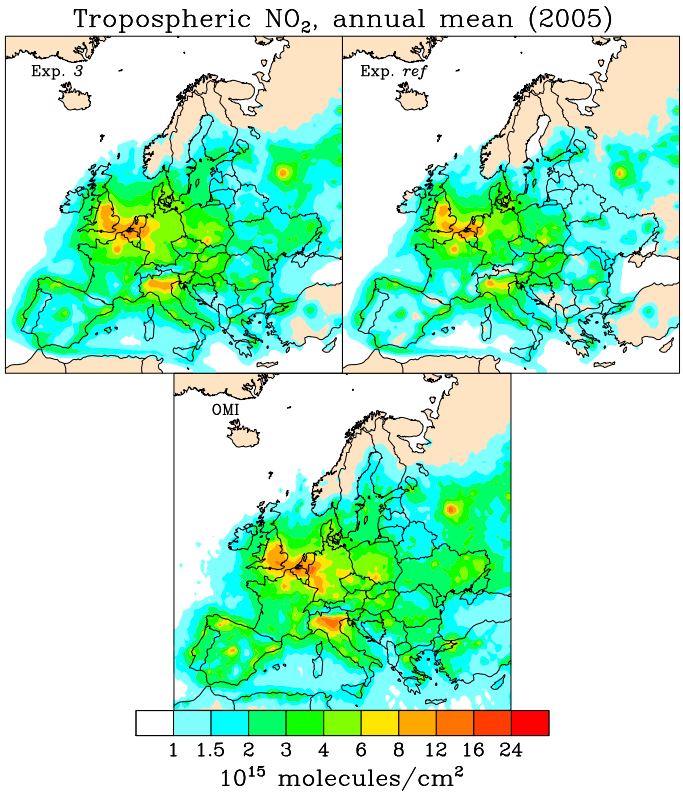

Fig. 5. Annual mean tropospheric NO_2 for experiments *ref* and *3* (upper panels), and corresponding OMI data (lower panels). The data shown were averaged as described in Sect. 3.3.

GMDD
5, 309–346, 2012

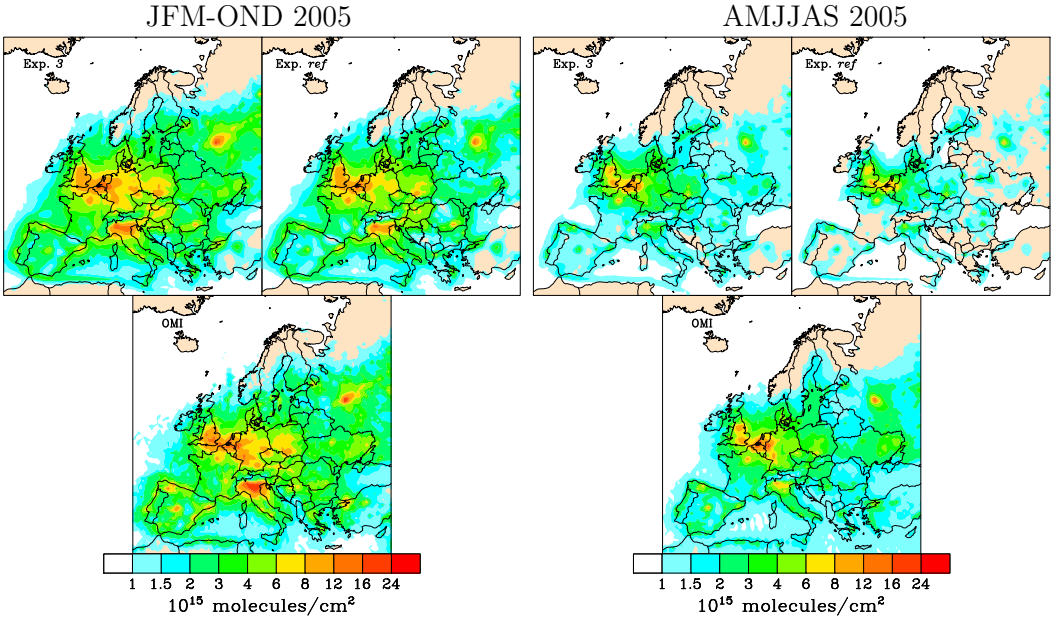

Fig. 6. Seasonally averaged tropospheric NO_2 for two six-month periods. See Fig. 5 for further details.

GMDD
5, 309–346, 2012

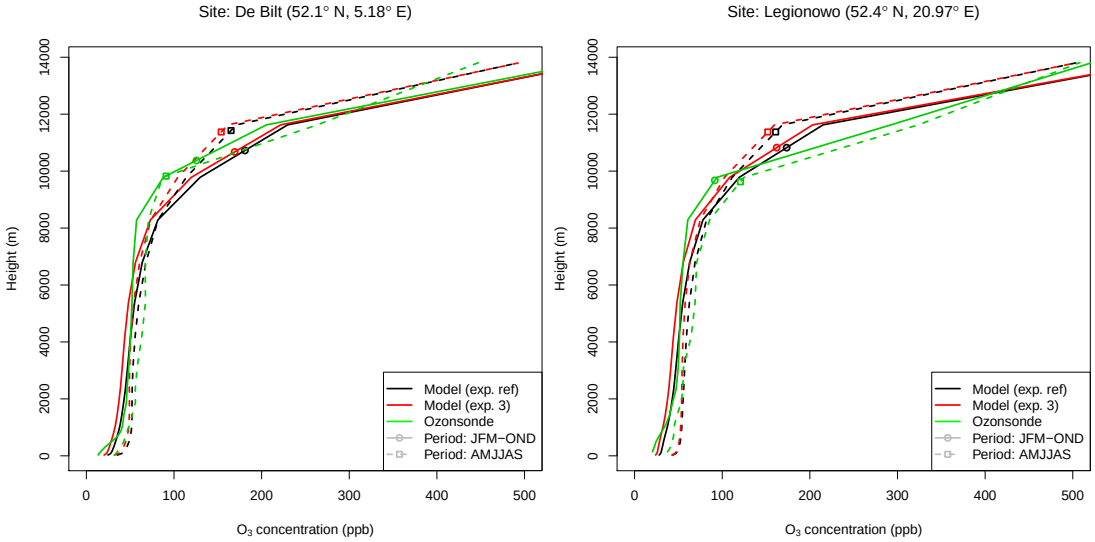

Fig. 7. Vertical profiles of O_3 concentrations at De Bilt (Holland) and Legionowo (Poland), as measured by ozonosondes and modelled by two simulations. These data were averaged over six month periods, and the line type (solid or dashed) indicates which period the averaging was taken over. The points correspond to the inferred O_3 tropopause height, according to the definition of Bethan et al. (1996). See Sect. 3.4 for further details.

GMDD
5, 309–346, 2012

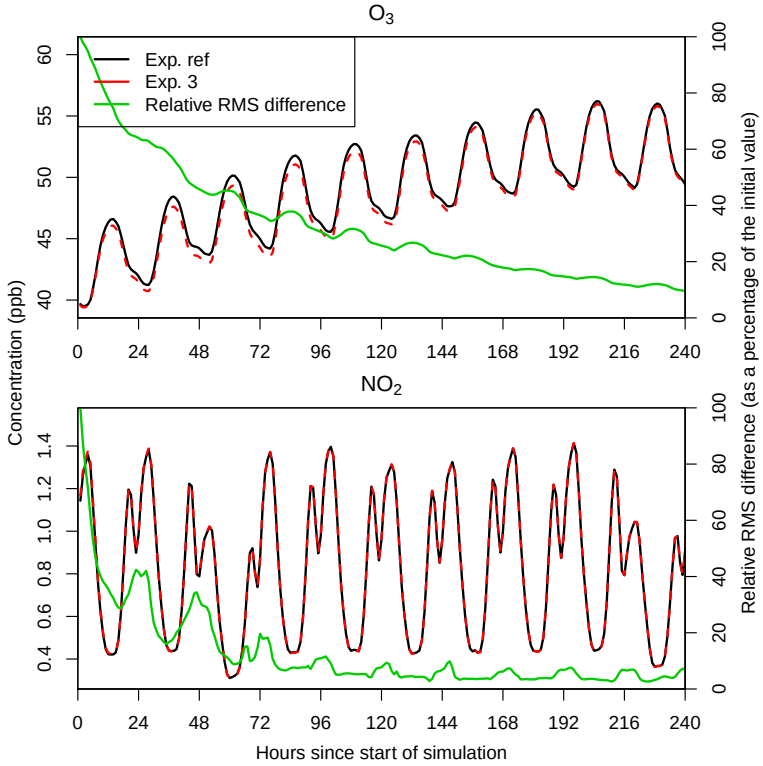

Fig. 8. Two simulations were initialised using concentration fields from two different experiments. This plot shows the mean concentration from the two simulations and the root mean squared (RMS) difference between the simulations (scaled relative to the RMS difference at the start of the simulation). These represent spatial averages of ground-level concentrations over the domain calculated for each hour. See Sect. 3.5 for further details.

GMDD
5, 309–346, 2012